Journal of Radiation Research, 2012, 53, 742–752
doi: 10.1093/jrr/rrs018 Advance Access Publication 5 July 2012

Automated estimation of number of implanted iodine-125 seeds for prostate brachytherapy based on two-view analysis of pelvic radiographs

Hidemichi KAWATA[1,*], Hidetaka ARIMURA[2], Hiroaki SUEFUJI[3], Sunao OHKURA[1], Yoshifumi SAIDA[1], Kazutaka NASHIKI[1], Kazuya HAYASHIDA[1], Tomomi KAWAHARA[1], Ayumu OHISHI[1] and Naofumi HAYABUCHI[3]

[1]Radiation Therapy Center, Kurume University Hospital, 67, Asahi-machi, Kurume, Fukuoka 830-0011, Japan
[2]Department of Health Sciences, Faculty of Medical Sciences, Kyushu University, 3-1-1, Maidashi, Higashi-ku, Fukuoka 812-8582, Japan
[3]Department of Radiology, School of Medicine, Kurume University, 67, Asahi-machi, Kurume, Fukuoka 830-0011, Japan
*Corresponding author. Radiation Therapy Center, Kurume University Hospital, 67, Asahi-machi, Kurume, Fukuoka 830-0011, Japan. Tel: +81-942-31-7647; Fax: +81-942-31-7647; Email:kawata@kurume.ktarn.or.jp

(Received 27 November 2011; revised 31 March 2012; accepted 3 April 2012)

Digital pelvic radiographs are used to identify the locations of implanted iodine-125 seeds and their numbers after insertion. However, it is difficult and laborious to visually identify and count all implanted seeds on the pelvic radiographs within a short time. Therefore, our purpose in this research was to develop an automated method for estimation of the number of implanted seeds based on two-view analysis of pelvic radiographs. First, the images of the seed candidates on the pelvic image were enhanced using a difference of Gaussian filter, and were identified by binarizing the enhanced image with a threshold value determined by multiple-gray level thresholding. Second, a simple rule-base method using ten image features was applied for false positive removal. Third, the candidates for the likely number of a multiply overlapping seed region, which may include one or more seeds, were estimated by a seed area histogram analysis and calculation of the probability of the likely number of overlapping seeds. As a result, the proposed method detected 99.9% of implanted seeds with 0.71 false positives per image on average in a test for training cases, and 99.2% with 0.32 false positives in a validation test. Moreover, the number of implanted seeds was estimated correctly at an overall recognition rate of 100% in the validation test using the proposed method. Therefore, the verification time for the number of implanted seeds could be reduced by the provision of several candidates for the likely number of seeds.

Keywords: prostate brachytherapy; estimation of number of iodine-125 seeds; pelvic radiographs; image processing in radiotherapy; two-view analysis

INTRODUCTION

The incidence of prostate cancer is rising rapidly not only in western countries but also in Asian countries, including Japan [1, 2]. About 32 000 deaths from prostate cancer were anticipated in the USA in 2010 [3], and about 10 000 deaths in Japan in 2007. A number of patients with early prostate cancer are treated by means of brachytherapy with permanent seed implants including iodine-125 seeds at low dose rates [4]. The advantage of this implant procedure is that there is sufficient dose coverage for localized prostate cancer, and reduction of harmful effects on healthy tissue. Furthermore, brachytherapy with iodine-125 seeds can preserve sexual function compared with external radiation and surgical prostatectomy [5–7].

The brachytherapy procedure with iodine-125 seeds consists of three steps: planning, implant of seeds and postoperative evaluation. The postoperative evaluation after

seed implantation is critical for validating the correct placement and the number of the implanted seeds according to preoperative or intraoperative planning, because seeds can migrate due to edema and swelling in the days immediately following their insertion [8, 9]. Seed migration could increase the probability of recurrence because of inadequate dose distribution in the prostate [10–13], and this could cause complications such as pulmonary and coronary artery embolization [14–18]. In this study, we did not deal with verification of correct placement of iodine-125 seeds; rather, this study focuses on estimation of the number of implanted seeds. The postoperative evaluation validating the number of the implanted seeds should be performed within a short time for the following two reasons: (i) a disagreement in the number of seeds between radiographs would be treated as an incidence of radiation source loss according to the Japanese Laws Concerning the Prevention of Radiation Hazards due to Radioisotopes and and; (ii)any adverse patient reactions to seed implantation, such as blood pressure reductions, body temperature decrease and hypopnea can be dealt with straight away in a hospital environment.

If the number of seeds on post-insertion pelvic radiographs of a patient does not agree with the true number of seeds, the patient cannot be moved out of the operating room. Therefore, the location and number of implanted seeds should be correctly and instantly identified just after seed insertion prior to moving the patient out of the operating room.

For this purpose, a number of automated identification methods for locating radioactive iodine-125 seeds and ascertaining the number of seeds for prostate brachytherapy have been developed based on three-dimensional (3D) reconstructed images by use of fluoroscopy images or digitized radiographs [19–21], computed tomography (CT) [22–24], magnetic resonance imaging (MRI) [25, 26] and tomosynthesis [27, 28]. However, it is difficult to employ imaging modalities such as CT or MRI in the operating room. Furthermore, since the 3D images are constructed using more than two views, obtained at different times, prostate displacement of the seeds due to motion and respiration can mean that they cannot be correctly detected [29, 30]. For that reason, two-view pelvic digital radiography is commonly used in clinical situations in Japan. However, it is difficult and laborious to visually and manually identify a large total number of implanted seeds (e.g. ~70) in digital radiographs within a short time span of 1 or 2 min, because the seeds are very small (around 1 mm diameter × 5 mm length), and two or more seeds often overlap in a projection image. Therefore, further studies on methods for automatically and immediately verifying the number of implanted seeds based on a simple radiograph are needed for assisting radiation oncologists or medical physicists in the postoperative evaluation procedure.

Our purpose in this research was to develop a fully automated method for estimation of the number of implanted iodine-125 seeds instantly prior to moving a patient out of the operating room, based on two-view analysis of pelvic radiographs, obtained just after seed insertion.

MATERIALS AND METHODS

Clinical cases

This study was approved by the Institutional Review Board (IRB) of our university hospital. We started to treat early-stage prostate cancer patients using iodine-125 brachytherapy from 2007. Twenty-eight patients (ages: 53–74 years, mean: 65 years) were selected from all patients from 2007 to 2009 in our university hospital, and this duration was approved by the IRB. All patients were treated with iodine-125 seeds (0.97 mm diameter × 4.55 mm length, OncoSeed GE Healthcare, Inc., Arlington Heights, USA). Fifty-six pelvic digital images of the 28 patients were acquired after seed implantation by a digital radiography (DR) system (Konica Minolta Health Care Co., Ltd, Tokyo, Japan) in two projections by use of an X-ray mobile C-arm (Toshiba Medical Systems Co., Ltd, Tokyo, Japan). The incidental X-ray angles were decided within an arbitrary ± 15° so there would be as little seed overlap as possible with the use of fluoroscopy and so as not to touch the patient or surgical table. The pelvic images were taken with an anti-scatter grid (grid ratio 5:1, grid density 34 lines/cm) at X-ray tube voltages of 80–90 kV and 10–20 mAsecond. The matrix size, pixel size and the number of gray levels in the pelvic DR images were 1430 × 1722, 0.175 mm, and 4096, respectively. Forty-nine pelvic radiographs were selected after excluding seven images, which had a lot of noise, blurred edges due to patient movement, and implanted seeds outside the irradiation field for this study. A total of3582 of the implanted iodine-125 seeds were visually confirmed in the 49 pelvic radiographs with consensus by two radiation oncologists and a medical physicist. The mean number of seeds was 73 per patient. For a validation test of our proposed method, we divided the 28 cases including 49 images into two groups, i.e. training and test images; the numbers of images were 21 and 28, respectively.

Automated identification of implanted seeds

Figure 1 shows a schematic diagram of the automated identification of implanted seeds. The seed candidates were identified using the following steps. First, a field of view with a circular shape was segmented by analysis of edge pixel-value profiles in the horizontal and vertical directions within the edge-enhanced image by a Sobel filter (mask size: 7 × 7 pixels). The Sobel filters in the horizontal and

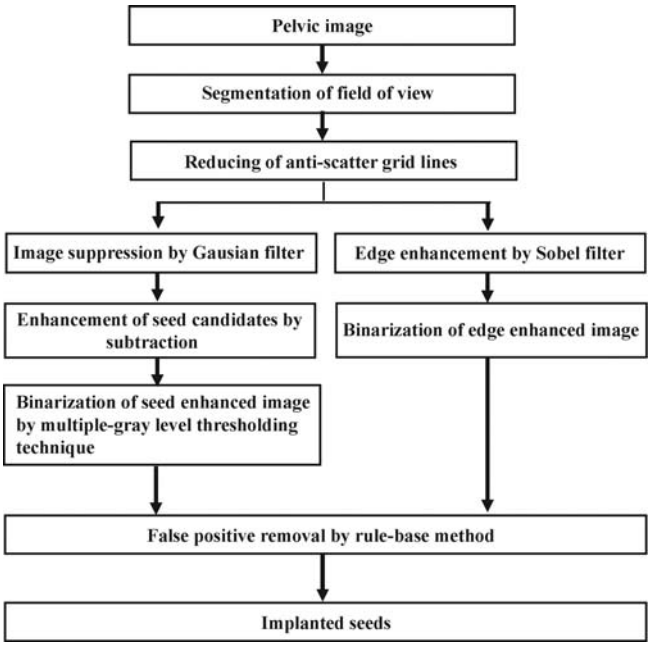

Fig. 1. Proposed scheme for automated identification of implanted seeds.

vertical directions used for this study were defined by:

$$f_x \begin{bmatrix} -1 & 0 & 0 & 0 & 0 & 0 & 1 \\ 0 & 0 & 0 & 0 & 0 & 0 & 0 \\ 0 & 0 & 0 & 0 & 0 & 0 & 0 \\ -2 & 0 & 0 & 0 & 0 & 0 & 2 \\ 0 & 0 & 0 & 0 & 0 & 0 & 0 \\ 0 & 0 & 0 & 0 & 0 & 0 & 0 \\ -1 & 0 & 0 & 0 & 0 & 0 & 1 \end{bmatrix}$$

$$f_y \begin{bmatrix} -1 & 0 & 0 & -2 & 0 & 0 & -1 \\ 0 & 0 & 0 & 0 & 0 & 0 & 0 \\ 0 & 0 & 0 & 0 & 0 & 0 & 0 \\ 0 & 0 & 0 & 0 & 0 & 0 & 0 \\ 0 & 0 & 0 & 0 & 0 & 0 & 0 \\ 0 & 0 & 0 & 0 & 0 & 0 & 0 \\ 1 & 0 & 0 & 2 & 0 & 0 & 1 \end{bmatrix}$$

The large mask size of 7×7 was employed for detection of large structure edges such as the irradiation field. Only magnitudes of the gradient vectors obtained by the Sobel filters were used in enhancement of the image edges. Second, anti-scatter grid lines on the image were suppressed by a low pass filter (below 0.56 mm^{-1}). Third, the images of the seeds were enhanced using a difference of Gaussian (DOG) filter, i.e. subtraction of a smoothed image with a Gaussian filter (mask size: 25×25 pixels, standard deviation: 17 pixels) from the suppressed grid-line image. The large Gaussian filter with a mask size of 25×25 pixels was used to suppress the implanted seeds as much as possible. Finally, numerous seed candidate regions were obtained by binarizing the enhanced seed image with a threshold value determined by use of a multiple-gray-level thresholding technique. The threshold value was determined so that the number of seed candidates would be smaller than 160. On the other hand, the edge-enhanced image with a Sobel filter (mask size: 7×7 pixels) was binarized by one of the three threshold values, which was automatically determined by one of the ratios of 0.06, 0.015 and 0.005 peak level in the pixel histogram based on the threshold value of the enhanced image of the seed. Each peak level was determined empirically in this study. The grid lines were suppressed by the low pass filter below 0.56 mm^{-1}. Figure 2 shows illustrations for segmentation of seed candidate regions based on the DOG filter and a multiple-grey level thresholding technique. By applying the DOG filter, i.e. subtraction of the Gaussian-smoothed image (Fig. 2b) from the grid line-suppressed image (Fig. 2a), background structures such as the pelvic bone, colon gas and the bladder were attenuated effectively with contrast medium, as shown in Fig. 2c, whereas the seed contrast became higher than that in the original image. Finally, as shown in Fig. 2d, seed candidate regions were segmented well, including some obvious false positive (FP) regions, by use of the multiple-gray-level thresholding technique. The binarized edge-enhanced images were used only for determination of region coincidence, which is one of the image features for FP removal.

False positive removal by a rule-based method

A simple rule-based method was applied for removal of seed FPs with use of nine image features, i.e. minimum,

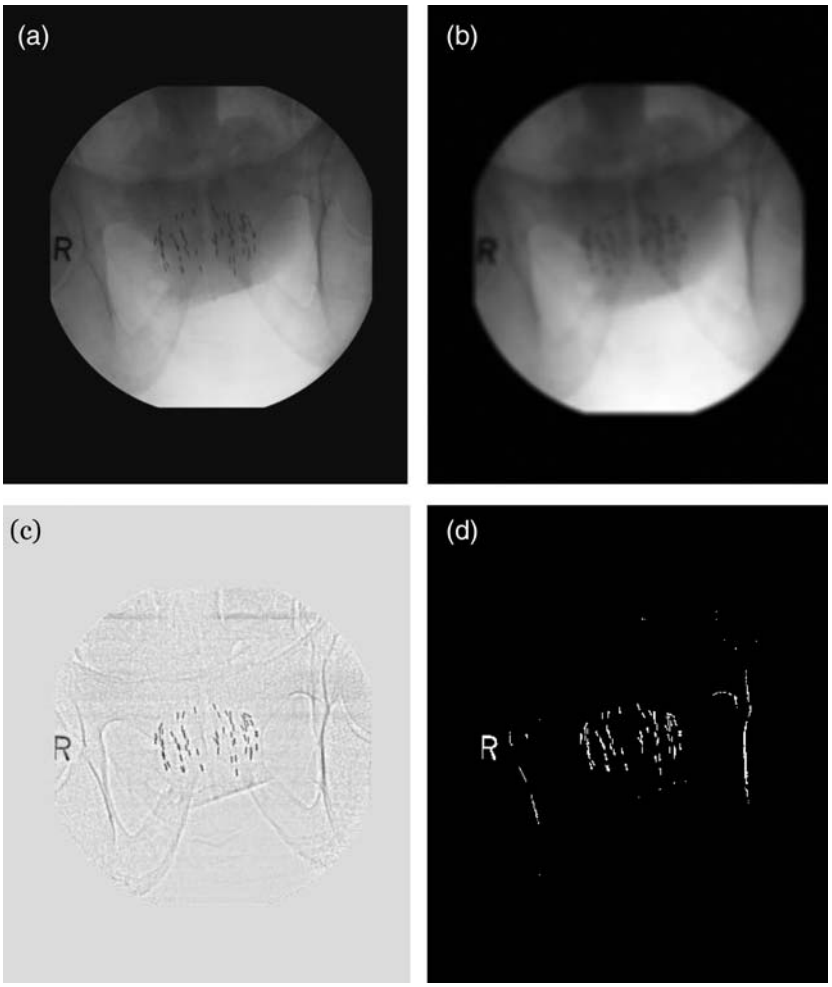

Fig. 2. Illustrations of segmentation of seed candidate regions: (**a**) a grid-line-suppressed image, (**b**) an image smoothed by a Gaussian filter, (**c**) an enhanced image of a seed, (**d**) seed candidate regions obtained by a multiple-gray-level thresholding technique.

maximum and mean pixel values and their SD, contrast in the enhanced seed image, area (the number of pixels), circularity, slenderness and region coincidence. Contrast was defined as the maximum pixel value minus the minimum pixel value in the seed candidate region. Circularity was defined as the ratio of the overlapping area of a seed candidate within the equivalent-area circle to the area of the seed candidate. Region coincidence was defined as the ratio of the logical AND region to the logical OR region between a binarized seed enhancement image and a binarized edge-enhancement image. Each rule for each image feature used in the rule-based scheme was based on a simple threshold value, which was determined from all true seed regions. The rules for the minimum and maximum pixel value were greater than each mean value plus 2 SD and 3 SD, respectively, and the rules for the mean pixel value, SD and contrast were less than each mean value minus 3 SD. Seed candidates with a number of pixels >50 and <1400 were removed as noise or large structures of pelvic bone or X-ray marker, respectively. The rule of the circularity for FP removal was below 10% or above 90%. Slenderness was defined as the number of times morphological erosion of a binary image was performed until the seed candidate disappeared, and the rule for FP removal was a value less than the mean minus 2 SD. The region coincidence rule for FP removal was <40%.

Outlier FP removal by accumulated profile analysis

The remaining outlier FPs on the bone edge, which exist outside a 'prostate' region, were removed by use of accumulated profiles based on the number of pixels in a binary image with segmented seed candidate regions in the horizontal and vertical directions. The 'prostate' region is where a prostate is supposed to be. Figure 3 shows accumulated profiles on the binary image in two directions. The bin width for producing the accumulated profile was set as

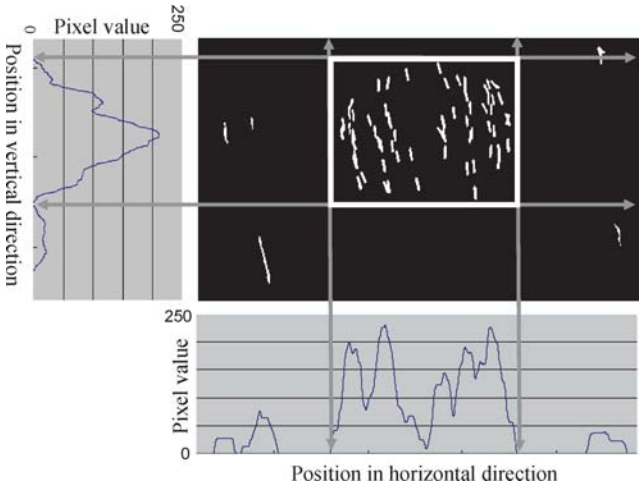

Fig. 3. Accumulated profiles on a binary image with segmented seed candidate regions in horizontal and vertical directions.

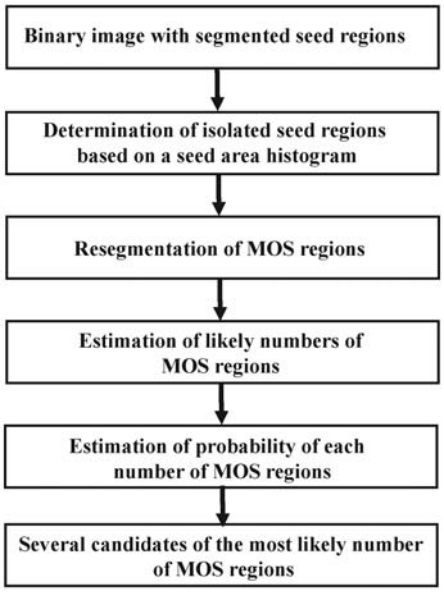

Fig. 4. Proposed scheme for automated estimation of the number of seed regions including isolated seed regions and multiply overlapping seed (MOS) regions.

70 pixels (12.25 mm) because the seeds were inserted at 10-mm intervals with use of a perineal template, and the magnification ratio of the seeds on an image was almost 1.2× in this radiographic geometry. The maximum value of the accumulated profile of each direction was detected, and then a circumscribed quadrangle around the 'prostate' was determined by four positions corresponding to four feet of two profile peaks <5% of the maximum value in the horizontal and vertical directions, as shown in Fig. 3. Finally, several outlier FPs outside the 'prostate' region were removed by use of the circumscribed quadrangle.

Performance evaluation of automated identification of implanted seeds

The center coordinates of all seeds on a pelvic image were determined by two radiation oncologists and a medical physicist, and considered as gold standards. A seed candidate was detected as true positive (TP) if the seed candidate region included the 'center' coordinate, but otherwise was considered as a false negative (FN).

Automated estimation of the number of implanted seeds

Figure 4 shows a proposed scheme for automated estimation of the number of implanted seeds. The candidates for the likely number of each region, which may include one or more seeds, were determined based on a seed candidate area histogram using the following six steps. Note that only true positive seeds were dealt with in this step.

(i) The number of isolated seeds was estimated from a major peak in a seed candidate area histogram.
(ii) The number of pixels in each multiply overlapping seed (MOS) region was corrected by consideration of the variation of pixel values on the periphery and overlapping areas in the MOS region.
(iii) The likely numbers of MOS regions including two or more seeds were calculated.
(iv) The probability of each number of overlapping seeds was estimated based on the frequency of the likely numbers of the seeds.
(v) The most likely candidates for the number of overlapping seeds were selected based on their higher probabilities in one-view analysis of pelvic radiograph.
(vi) The most likely candidates for the number of overlapping seeds were selected based on their higher probabilities in two-view analysis of pelvic radiographs.

Estimation of the number of isolated seeds based on seed candidate area histograms

Figure 5 shows an example of the seed candidate area histogram for all cases used in this study. The seed candidate area histogram was used for classifying all seed candidates into isolated seeds and overlapping seeds, and for calculating the mean and SD of isolated seeds area. We assumed that the seed regions smaller than a threshold area at the largest peak of the seed candidate area histogram were considered as isolated seeds. That is because originally all seeds were individually implanted within a prostate, and thus the largest peak is considered to include a majority of isolated seeds.

Correction of the number of pixels in a region with MOS

Basically, the number of seeds in an MOS region is estimated by dividing a predicted number of pixels within the MOS region by the mean area of the isolated seed regions. However, there are two requirements for more accurate estimation of the number of seeds in the MOS region if the number is estimated in one of the projection images as follows: Requirement (i) each MOS region should be resegmented because the pixel values on the periphery of the MOS region vary with the seed location, tube voltage or abdominal thickness, and thus the contrast of each MOS region to the background in a projection image could change with such factors; and (ii) Requirement (ii) we need to count the number of pixels in an overlapping area twice by identifying the overlapping area in one projection of the pelvic image with implanted seeds. For example, if the number of pixels in a region with two overlapping seeds was estimated in a projection image, the number of pixels in the overlapping seed region would be smaller than twice the mean area of the isolated seed regions due to an overlapping area between the two seeds.

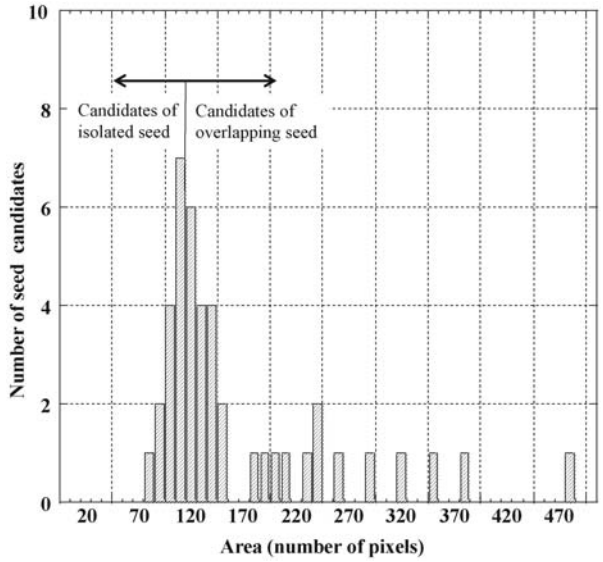

Fig. 5. Seed candidate area histogram for all cases used in this study. The seed regions smaller than a threshold area at the largest peak of this histogram were considered as isolated seeds.

Therefore, the number of pixels in the MOS regions obtained by the multiple-gray level thresholding explained in the section on 'Identification of initial seed candidate regions' was corrected using the following method. Figure 6 shows the correction of the number of pixels in an MOS region based on the following two steps. In the first step for Requirement (i), a threshold value was determined for each MOS region by changing the mean pixel value of the isolated seeds plus $\beta \times SD$, where β was changed from 0.1 to 5.5 in increments of 0.1, until the average incremental number of pixels for all MOS regions was equal to the average number of pixels on the peripheral lengths of all isolated seeds. Then, all MOS regions were resegmented by the threshold value as shown in Figure 6c. In the second step for Requirement (ii), the overlapping areas were identified based on a thinned image for each MOS region. Let us consider the case where a seed overlaps with another seed. In this instance, the pixel values on the centerline, which correspond to an overlapping area between the two seeds, are slightly lower than those on the centerline where they are not overlapping in an enhanced seed image. Therefore,

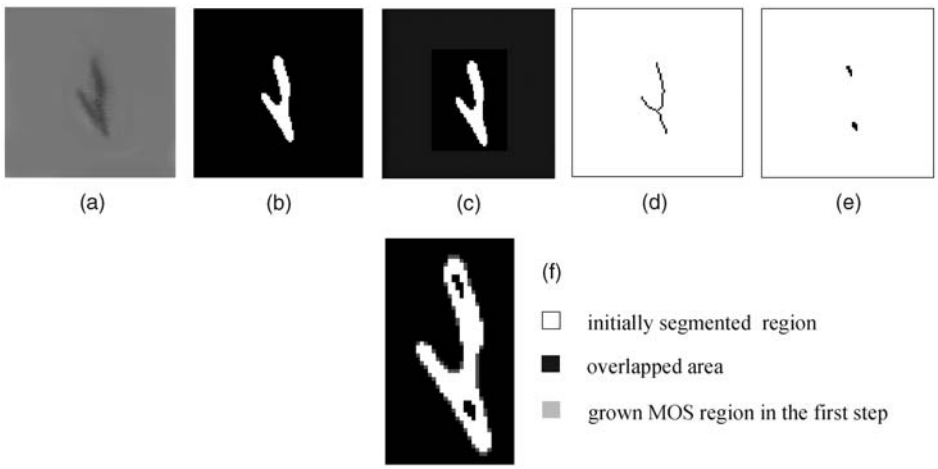

Fig. 6. Correction of the number of pixels in a multiply overlapped seed (MOS) region: (**a**) an enhanced image of a seed with an MOS region including five seeds, (**b**) an initially segmented MOS region derived from multiple-gray level thresholding, (**c**) a grown MOS region in the first step, (**d**) a thinned image derived from the initial MOS region (b), (**e**) a segmented overlapped area in the second step and (**f**) an image including the results of the two steps.

a thinned image was obtained for determination of centerlines from the initially segmented MOS region by multiple-gray-level thresholding. Next, pixels, which are lower than the mean pixel value minus the SD on the centerlines, are considered as pixels in overlapping areas. Finally, the number of such pixels is counted twice.

Figure 6a shows an enhanced seed image with an MOS region including five seeds. Some areas, which may be overlapping areas, are darker than other areas. Figure 6d shows a thinned image derived from the initial MOS region, shown in Fig. 6b. Figures 6e and f show a segmented overlapping area in the second step and an image including all results in the two steps.

Estimation of the likely number of overlapping seeds based on one-view analysis of pelvic radiograph

The probability $P(x)$ of likely numbers x of overlapping seeds including two or more was defined by the frequency of the number of seeds determined from the candidate area divided by the mean area of isolated seeds with changing SDs. The probability was calculated for each MOS region using the following algorithm:

Step 1: Setting α and *Nc* as –4.0 and 0, respectively, and calculation of the average area of the isolated seeds.

Step 2: Increment of α and *Nc* by 0.1 and 1, respectively.

Step 3: Calculation of the likely number x of overlapping seeds using the following equation:

$$x = \left[\frac{A_c}{A + \alpha\sigma}\right]$$

where [ ] is the floor function, A_c is the candidate area and A_1 is the isolated candidate area.

Step 4: Count of the frequency *Nx* of each likely number of overlapping seeds.

Step 5: If $\alpha > 4.0$, the probabilities of all candidates of the likely number x of overlapping seeds are calculated by *Nx/Nc*.

If not, go to **Step 2**.

Several candidates for the most likely number of the overlapping seeds were selected based on their higher probabilities. Figure 7 shows an example histogram of the likely numbers of an MOS region including five overlapping seeds. To evaluate this estimation method of the likely number of overlapping seeds, the recognition rate was calculated by dividing the estimated number of seeds by the true number of implanted seeds, which was determined by two radiation oncologists and a medical physicist.

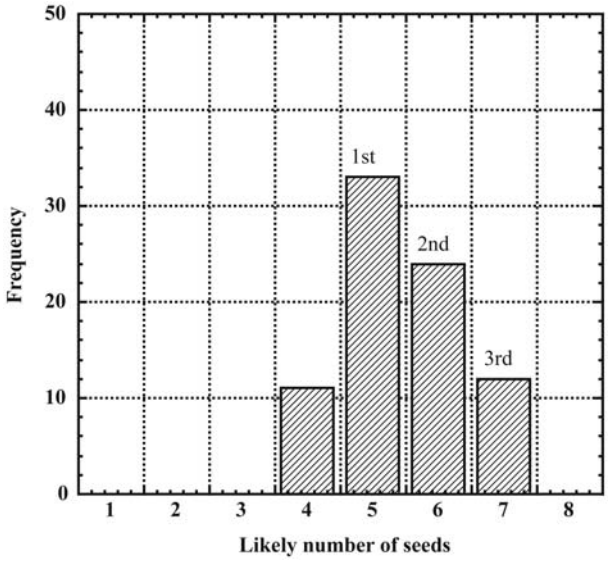

Fig. 7. Example of a histogram of the likely numbers of an MOS region including five overlapping seeds.

Estimation of the likely number of overlapping seeds based on two-view analysis of pelvic radiographs

The final numbers of overlapping seeds were estimated based on two-view analysis of pelvic radiographs. Because the regions of all overlapping seeds on two pelvic radiographs did not agree with each other, the location and number of regions of overlapping seeds are inconsistent with each other. Therefore, we adopted two-view analysis of pelvic radiographs based on two results of one-view analysis of pelvic radiographs in two directions. The most likely five candidates for the number of overlapping seeds were selected from all candidates of the most likely number of the overlapping seeds, which were determined based on the one-view analysis of the two pelvic radiographs of a patient. With this method, six patients were employed as a training data set and a test data set, respectively.

The candidate for total number of all implanted seeds was detected as a TP if the candidate, which was selected by its higher probability, included the true number of implanted seeds in either result of the two-view analysis of pelvic radiographs, but otherwise was an FN. The overall recognition rates of the number of implanted seeds were calculated by dividing the number of TPs by the number of patients.

RESULTS

The evaluation was based on two-step evaluations, i.e. (i) the sensitivity of seed locations and (ii) the recognition rate of the isolated seeds and the likely number of overlapping seeds for TP seeds. All procedures took 224.1 ± 30.3 s to carry out using a central processing unit (CPU) on a

personal computer with a 2.53-GHz-CPU (Intel Core 2 Duo) 4-GB random access memory (RAM). The proposed method detected 99.9% (1508/1510) of implanted seeds with 0.71 FP per image on average in a test for training cases. Table 1 shows the results of automated identification of implanted seeds in the training cases and the test cases. Twenty-four false positives were detected on the pubic bones and urethra catheters, and eighteen seeds in very-low-contrast regions were missed. All isolated seed candidates (544) were correctly identified as one seed. Figure 8 shows the relationship between the number of candidates for the most likely number of seed regions and the recognition rate of the automated estimation in the training cases and the test cases. The recognition rate of overlapping seeds was 72.4% when we used the first candidate of the likely number of overlapping seeds in the training cases. If the most likely three candidates of the number of overlapping seeds were selected, the correct number of seeds for all regions was included in the three candidates with a recognition rate of 97.5% (Fig. 8a).

Table 1. Results of automated identification of implanted seeds in the training cases and the test cases

Training cases				Test cases			
Image number	**Number of seeds**	**False positive**	**False negative**	**Image number**	**Number of seeds**	**False positive**	**False negative**
1	65	0	0	1	65	0	0
2	65	0	0	2	65	0	0
3	90	0	0	3	65	0	1
4	90	0	0	4	65	2	0
5	83	0	0	5	79	0	0
6	83	0	0	6	79	1	0
7	75	0	0	7	75	1	2
8	75	0	0	8	75	0	0
9	55	0	0	9	55	0	0
10	55	2	0	10	55	0	0
11	70	0	0	11	73	3	0
12	90	0	0	12	73	0	12
13	90	0	0	13	103	1	0
14	65	0	0	14	72	0	0
15	65	0	0	15	72	0	0
16	68	0	0	16	99	0	0
17	68	3	2	17	75	0	0
18	60	6	0	18	75	0	0
19	60	0	0	19	84	0	0
20	69	0	0	20	60	1	0
21	69	4	0	21	90	0	0
				22	60	0	0
				23	60	0	1
				24	63	0	0
				25	85	0	0
				26	85	0	0
				27	83	0	0
				28	83	0	0
Total	1510	15	2	Total	2073	9	16

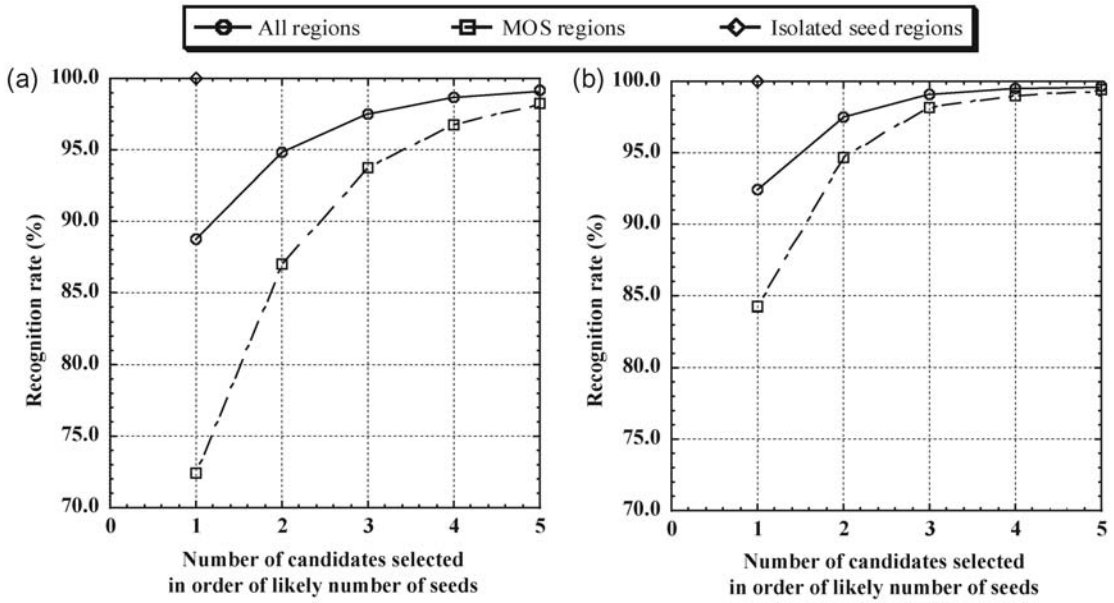

Fig. 8. Relationship between the number of candidates for the most likely number of seed regions and the recognition rate of automated estimation: (**a**) training cases, and (**b**) test cases.

In the test cases, the sensitivity of identification of implanted seeds was 99.2% (1982/2073) with 0.32 FP per test image as shown in Table 1. All isolated seeds (515) were identified correctly. The recognition rate for all regions was 92.4% using only the first candidate for the likely number of overlapping seeds, and 99.1% using three candidates for the likely number.

Figure 9 shows the relationship between the number of candidates for the most likely number of all implanted seeds and the overall recognition rate based on two-view analysis of pelvic radiographs. The overall recognition rate was up to 83.3% at the fourth or fifth candidate for number of all implanted seeds in the training cases, and was 100.0% for the third candidate in the test cases.

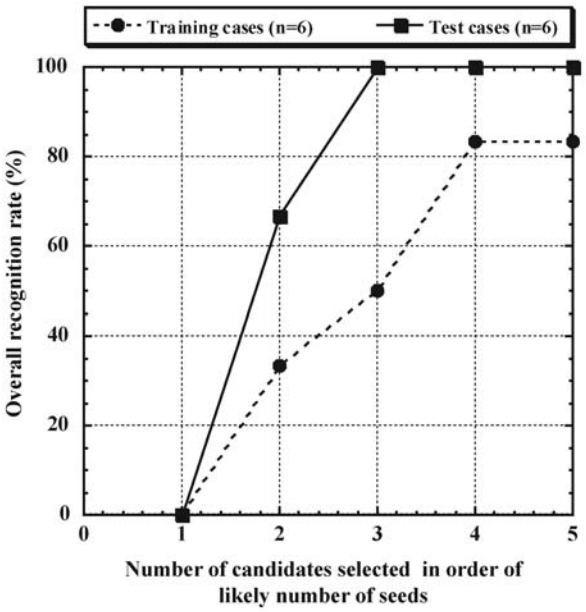

Fig. 9. Relationship between the number of candidates for the most likely number of seed regions and the overall recognition rate with two-projection pelvic images analysis.

DISCUSSION

Tubic *et al.* [19] developed an automated method for the detection of the position and the orientation of implanted seeds on fluoroscopic images or scanned radiographs. They reported that the sensitivity for detection of implanted seeds was 92.0% using their method. Su *et al.* [20] developed a method of determination of 3D seed positions from multiple radiographic projections by dealing with overlap of seed images. Their method produced 3.0 FPs with a sensitivity of 98% in a phantom study (implanted 64 seeds), based on 3D reconstruction of three projections of fluoroscopic images. Benkhoucha *et al.* [28] developed an automatic tomosynthesis-based seed detection technique, which yielded seed a detection rate of 96.7% and 2.6% FPs. Whitehead *et al.* [24] proposed a technique for localizing brachytherapy seeds by utilizing voxel intensity, which would provide seed detection and localization especially for low resolution CT data sets. In four separate simulations (X-ray CT images of three separate phantoms containing multiple implanted seeds in different configurations, and in an *in vivo* X-ray CT volume data set), all simulated seed

objects were detected. On the other hand, our proposed method detected 99.9% of implanted seeds with 0.71 FPs per image on average in a test for training cases (21 clinical images), and 99.2% with 0.32 FPs in a validation test (28 clinical images). Therefore, the detection sensitivity seems to be comparable with the past studies, and the number of false positives is improved.

Eighteen seeds (0.5%), which were overlapping with anatomic regions or materials such as pubic bone or a catheter, were missed by the automated identification of implanted seeds in the proposed method. Especially, in a radiograph of one particular patient (#12), 12 FNs occurred in lower contrast regions where the pubic symphysis and the bladder with contrast media were overlapping with implanted seeds. In addition, the edges of the pelvic bone, as well as parts of the pubic symphysis and pelvic cavity, were detected as 0.32 FPs per image because of their similarity to implanted seeds. Therefore, we should improve the automated seed identification method in terms of the detection of seeds and removal of FPs in future work.

The overall recognition rate of number of implanted seeds in the test cases was 100% using two-view analysis of pelvic radiographs, if three candidates were selected for the likely number. Therefore, it is possible to use this technique for final verification of the number of implanted seeds. Furthermore, the proposed method may reduce the radiologists' workloads in a clinical situation, as radiologists would only have to count the number of isolated seeds, but they should verify the numbers of multiply overlapping seeds. The overall recognition rate could be improved if using several projection images (three or more) taken at various angles [21], but patient dose and labor for radiography would be increased compared with this study. Our proposed method, based on two-view analysis of pelvic radiographs, gave a good estimate of the number of implanted seeds with minimal patient dose and labor for radiography.

As shown in Fig. 8b, all candidates for the most three likely numbers estimated by the proposed method were incorrect for 0.9% of overlapping seeds in the test cases.

In this study, three candidate numbers for each MOS region with more than one seed were selected based on the three highest probabilities. This depends on the segmentation accuracies of overlapping seed regions and isolated seed regions. Furthermore, some of the overlapping seed regions were not segmented well, and the most likely candidate numbers tended to be incorrect. Therefore, we should improve the segmentation method for the overlapping seed regions in future work.

We recognize that there are two limitations in the proposed method. First, the users of the proposed method have to select one of no more than three candidate numbers for the multiply overlapping seeds produced by the proposed method. This would not be practical in a clinical situation. One possibility to overcome this would be to verify whether the 'true' number of seeds, which the radiologist implanted, is included in the list of candidate numbers of implanted seeds suggested by the proposed method. Second, there is an average computation time of about 4 min, which may be relatively long for clinical use, but as the time could be greater shortened to <30 s if graphical processing units (GPUs) were to be employed. In addition, we should improve the algorithm of the proposed method with respect to efficient computation.

CONCLUSIONS

Because a disagreement in the number of seeds between radiographs would be treated as an incidence of radiation source loss according to the Japanese Laws Concerning the Prevention of Radiation Hazards due to Radioisotopes and Others, we need an automated method for verifying the number of seeds within a short time. Therefore, we have developed an automated method for estimation of the numbers of implanted iodine-125 seeds on a pelvic radiograph after permanent prostate implants. The proposed method detected 99.2% of implanted seeds with 0.32 false positives in a validation test. If the most likely three candidates for the number of implanted seeds were selected, the number of implanted seeds was estimated correctly at an overall recognition rate of 100% in the validation test. Therefore, the preliminary results showed that the proposed method would be useful for estimation of the numbers of implanted seeds on pelvic radiographs with a high rate of seed detection and recognition of the number of seeds. Furthermore, the proposed method would be simple to apply in clinical situations Justas it only requires two-view pelvic radiographs.

REFERENCES

1. Hsing WA, Tsao L, Devesa S. International trends and patterns of prostate cancer incidence and mortality. *Int J Cancer (Pred. Oncol)* 2000;**85**:60–7.
2. Matsuda T, Marugame T, Kamo K *et al*. The Japan Cancer Surveillance Research Group. Cancer incidence and incidence rates in Japan in 2002: based on data from 11 population-based cancer registries. *Jpn J Clin Oncol* 2008;**38**:641–8.
3. American Cancer Society. *Cancer Facts and Figures 2010*. Atlanta, GA: American Cancer Society 2010, 23–37.
4. Stone NN, Stock RG. Permanent seed implantation for localized adenocarcinoma of the prostate. *Current Urology Reports* 2002;**3**:201–6.
5. Downs TM, Sadetsky N, Pasta DJ *et al*. Health related quality of life patterns in patients treated with interstitial prostate brachytherapy for localized prostate cancer – data from CAPSURE. *J Urol* 2003;**170**:1822–27.
6. Buron C, Le Vu B, Cosset JM *et al*. Brachytherapy versus prostatectomy in localized prostate cancer: result of a French

multicenter prospective medico-economic study. *Int J Radiat Oncol Biol Phys* 2007;**67**:812–22.
7. Wei JT, Dunn RL, Sandler HM *et al*. Comprehensive comparison of health-related quality of life contemporary therapies for localized prostate cancer. *J Clin Oncol* 2002;**20**:557–66.
8. Chen Z, Yue N, Wang X *et al*. Dosimetric effects of edema in permanent prostate seed implants: a rigorous solution. *Int J Radiat Oncol Biol Phys* 2000;**47**:1405–19.
9. Kono Y, Kubota K, Aruga T *et al*. Swelling of the prostate gland by permanent brachytherapy may affect seed migration. *Jpn J Clin Oncol* 2010;**40**:1159–65.
10. Fuller DB, Koziol JA, Feng AC. Prostate brachytherapy seed migration and dosimetry: analysis of stranded sources and other potential predictive factors. *Brachytherapy* 2004;**3**:10–19.
11. Gao M, Wang JZ, Nag S *et al*. Effects of seed migration on post-implant dosimetry of prostate brachytherapy. *Med Phys* 2007;**34**:471–80.
12. Wuu CS, Ennis RD, Schiff PB *et al*. Dosimetric and volumetric criteria for selecting a source activity and a source type (125I or 103Pd) in the presence of irregular seed placement in permanent prostate implants. *Int J Radiat Oncol Biol Phys* 2000;**47**:815–20.
13. Al-Qaisieh B, Witteveen T, Carey B *et al.* Correlation between pre-and postimplant dosimetry for Iodine-125 seed implants for localized prostate cancer. *Int J Radiat Oncol Biol Phys* 2009;**75**:626–30.
14. Tapen EM, Blasko JC, Grimm PD *et al*. Reduction of radioactive seed embolization to the lung following prostate brachytherapy. *Int J Radiat Oncol Biol Phys* 1998;**42**:1063–7.
15. Eshleman JS, Davis BJ, Pisansky TM *et al*. Radioactive seed migration to the chest after transperineal interstitial prostate brachytherapy: extraprostatic seed placement correlates with migration. *Int J Radiat Oncol Biol Phys* 2004;**59**:419–25.
16. Fukada J, Yorozu A, Toya K *et al*. Pulmonary embolization of permanently implanted radioactive iodine-125 seeds for carcinoma of the prostate. *Nippon Acta Radiologica* 2005;**65**:121–3.
17. Zhu AX, Wallner KE, Frivold GP *et al*. Prostate brachytherapy seed migration to the right coronary artery associated with an acute myocardial infarction. *Brachytherapy* 2006;**5**:262–5.
18. Davis BJ, Bresnahan JF, Stafford SL *et al*. Prostate brachytherapy seed migration to a coronary artery found during angiography. *J Urol* 2002;**168**:1103.
19. Tubic D, Zaccarin A, Pouliot J *et al*. Automated seed detection and three-dimensional reconstruction. I. Seed localization from fluoroscopic images or radiographs. *Med Phys* 2001;**31**:1277–87.
20. Su Y, Davis BJ, Herman MG *et al*. Prostate brachytherapy seed localization by analysis of multiple projections: Identifying and addressing the seed overlap problem. *Med Phys* 2004;**28**:2265–71.
21. Jain AK, Zhou Y, Mustufa T *et al*. Matching and reconstruction of brachytherapy seeds using the Hungarian algorithm (MARSHAL). *Med Phys* 2005;**32**:3475–92.
22. Prestidge BR, Bice WS, Kiefer EJ *et al*. Timing of computed tomography-based postimplant assessment following permanent transperineal prostate brachytherapy. *Int J Radiat Oncol Biol Phys* 1998;**40**:1111–15.
23. Holupka EJ, Burdette EC, Kaplan ID. An automatic seed finder for brachytherapy CT postplans based on the Hough transform. *Med Phys* 2004;**31**:2672–79.
24. Whitehead G, Chang Z, Ji J. An automated intensity-weighted brachytherapy seed localization algorithm. *Med Phys* 2007;**35**:818–27.
25. Dubois DF, Prestidge BR, Hotchkiss LA *et al*. Source localization following permanent transperineal prostate interstitial brachytherapy using magnetic resonance imaging. *Int J Radiat Oncol Biol Phys* 1997;**39**:1037–41.
26. Bloch BN, Lenkinski RE, Helbich TH *et al*. Prostate postbrachytherapy seed distribution: comparison of high-resolution, contrast-enhanced, T1- and T2-weighted endorectal magnetic resonance imaging versus computed tomography: initial experience. *Int J Radiat Oncol Biol Phys* 2007;**69**:70–8.
27. Tutar IB, Managuli R, Shamdasani V *et al*. Tomosynthesis-based localization of radioactive seeds in prostate brachytherapy. *Med Phys* 2003;**30**:3135–42.
28. Brunet-Benkhoucha M, Verhaegen F, Lassalle S *et al*. Clinical implementation of a digital tomosynthesis-based seed reconstruction algorithm for intraoperative postimplant dose evaluation in low dose rate prostate brachytherapy. *Med Phys* 2009;**36**:5235–44.
29. Tubic D, Zaccarin A, Beaulieu L *et al*. Automated seed detection and three-dimensional reconstruction.II. Reconstruction of permanent prostate implants using annealing. *Med Phys* 2001;**28**:2272–9.
30. Lam ST, Cho PS, Marks RJ II *et al*. Detection and correction of patient movement in prostate brachytherapy seed reconstruction. *Phys Med Biol* 2005;**50**:2071–87.